Available online at www.sciencedirect.com
SCIENCE DIRECT
International Journal of Heat and Mass Transfer 49 (2006) 1647–1657
International Journal of HEAT and MASS TRANSFER
www.elsevier.com/locate/ijhmt

Electrohydrodynamic enhancement of in-tube convective condensation heat transfer

H. Sadek [a], A.J. Robinson [a], J.S. Cotton [b], C.Y. Ching [a,*], M. Shoukri [a]

[a] McMaster University, Department of Mechanical Engineering, Hamilton, Ont., Canada
[b] Dana Corporation, Long Manufacturing Division, Oakville, Ont., Canada

Received 22 October 2004; received in revised form 25 October 2005
Available online 4 January 2006

Abstract

An experimental investigation of electrohydrodynamic (EHD) augmentation of heat transfer for in-tube condensation of flowing refrigerant HFC-134a has been performed in a horizontal, single-pass, counter-current heat exchanger with a rod electrode placed in the centre of the tube. The effects of varying the mass flux (55 kg/m^2 s $\leqslant G \leqslant$ 263 kg/m^2 s), inlet quality ($0.2 \leqslant x_{in} \leqslant 0.83$) and the level of applied voltage (0 kV $\leqslant V \leqslant$ 8 kV) are examined. The heat transfer coefficient was enhanced by a factor up to 3.2 times for applied voltage of 8 kV. The pressure drop was increased by a factor 1.5 at the same conditions of the maximum heat transfer enhancement. The improved heat transfer performance and pressure drop penalty are due to flow regime transition from stratified flow to annular flow as has been deduced from the surface temperature profiles along the top and bottom surfaces of the tube.

1. Introduction

There has been significant interest in condensation heat transfer enhancement techniques due to the advantages it offers in terms of increased performance and the possibility of more compact heat exchanger designs. Among the various enhancement techniques, the use of electrohydrodynamics (EHD) is appealing because it is relatively non-intrusive and provides a means of active control of the heat transfer. EHD augmentation involves the application of an electric field which interacts with the dielectric fluid medium to induce secondary motions that destabilize the thermal boundary layer near the heat transfer surface creating increased turbulence or bulk mixing of the flow and/or phases. This can lead to heat transfer coefficients that are several times higher than those achieved by more conventional enhancement techniques. The gain in the heat transfer performance is often large enough to offset any penalty resulting from the increase in pressure drop due to the application of EHD.

There have been several studies on EHD heat transfer enhancement during condensation and detailed reviews are given by Allen and Karayiannis [1] and Seyed-Yagoobi and Bryan [2]. The majority of the early studies on EHD condensation heat transfer have focused on the effect that a high voltage electric field has on free falling liquid films during condensation on vertical plates as well as both external and internal condensation on vertical tubes. Velkoff and Miller [3], Choi and Reynolds [4], Choi [5], Didkovsky and Bologa [6], Joos and Snaddon [7], Bologa et al. [8], Yabe et al. [9–11], Yamashita et al. [12], Wawzyniak and Sayed-Yagoobi [13], and Cheung et al. [14] investigated EHD augmented condensation on vertical surfaces. In these studies, a 1.6–20-fold increase in the heat transfer coefficient was obtained. The wide range of enhancement is primarily attributed to the diversity in the electrode/heat transfer surface configuration and geometry, the working fluids tested and applied voltage levels. The lowest range of enhancement is typical for in-tube condensation with co-axial electrodes [4,5,7]. There have been relatively fewer

* Corresponding author. Tel.: +1 905 525 9140; fax: +1 905 572 7944.
E-mail address: chingcy@mcmaster.ca (C.Y. Ching).

0017-9310/$ - see front matter © 2005 Elsevier Ltd. All rights reserved.
doi:10.1016/j.ijheatmasstransfer.2005.10.030

Nomenclature

c_p	specific heat at constant pressure (kJ/kg K)
E	electric field strength (V/m)
E_o	electric field strength (V/m)
G	mass flux (kg/m^2 s)
h	heat transfer coefficient (W/m^2 K)
I	current (A)
P_R	test section refrigerant inlet pressure (Pa)
Q	rate of heat transfer (W)
q''	heat flux (W/m^2)
S	surface area (m^2)
T	temperature (°C)
V	voltage (V)
x	vapor quality, distance from test section inlet
M_d	Masuda number $\left(=\frac{\varepsilon_o E_o T_o (\partial \varepsilon_s/\partial T)_\rho L^2}{2\rho_o v^2}\right)$

Greek symbols

ε	dielectric permittivity (N/V^2)
ε_o	dielectric permittivity of free space (N/V^2)
ρ	mass density (kg/m^3)
ρ_e	charge density (C/m^3)
α	void fraction
μ	dynamic viscosity (kg/ms)

Subscripts

cond	condenser
surr	gained from surroundings
i	inlet or inner
o	without EHD
PRE	preheater
R, ref	refrigerant
s	surface
w	water
l	liquid
v	vapor

investigations on the effect of EHD on free falling liquid films during condensation on horizontal or inclined heat transfer surfaces. Holmes and Chapman [15], Cooper and Allen [16], and Cheung et al. [14] among others, have contributed to knowledge in this area of EHD enhanced heat transfer. Enhancement ratios between 1.1 and 5.5 have been achieved for this heat transfer surface configuration.

The recent work of Singh [17], Gidwani et al. [18], and Feng and Seyed-Yagoobi [19] investigated the effect of EHD on in-tube convective condensation heat transfer. Singh [17] reported a 6.4-fold improvement in the condensation heat transfer for experiments of different flow regimes and electrode designs. However, it was found that the EHD introduces a pressure drop penalty due to additional frictional losses. An experimental study of EHD enhanced in-tube condensation of alternative refrigerants in both smooth and corrugated tubes was conducted by Gidwani et al. [18]. The authors reported a maximum enhancement of 18.8-fold with a corresponding pressure drop penalty of 11.8-fold with R404a as the working fluid. Feng and Seyed-Yagoobi [19] analyzed the effects of the electric fields on the heat transfer and the pressure drop in an annular two-phase flow. Furthermore, a theoretical model was developed to predict the heat transfer enhancement and the pressure drop penalty for horizontal annular two-phase flow in the presence of a radial electric field. The model predictions were found to be in good agreement with the experimental data for horizontal internal convective boiling of Singh [17], and Bryan and Seyed-Yagoobi [20] and the condensation experiments of Singh [17] for high mass flux.

Previous research in the field of EHD augmented two-phase flow has shown that the electric field induces an additional electrical body force on the flowing fluids. The general expression of the electric body force is [21,22]

$$f_e = \rho_e \overline{E} - \frac{1}{2}E^2\nabla\varepsilon + \frac{1}{2}\nabla\left[E^2\rho\left(\frac{\partial\varepsilon}{\partial\rho}\right)_T\right] \quad (1)$$

The three terms on the right-hand side of Eq. (1) represent the *electrophoretic*, *dielectrophoretic*, and *electrostrictive* components of the electric force respectively. The electrophoretic component represents the force acting on the free charge in the presence of an electric field, also known as the Coulomb force. This force usually dominates for adiabatic single-phase flow under the application of direct current. The dielectrophoretic component represents the force due to the spatial change of the permittivity of the dielectric medium as a result of temperature gradients and/or differences in the phases. The dielectrophoretic force is weaker than the electrophoretic force for adiabatic single-phase flow as the permittivity of the working fluid is a weak function of the electric field. If two phases exist, such as in convective boiling and condensation, the dielectrophoretic force will dominate and can have significant influence on the flow and heat transfer behavior. The electrostrictive force is caused by the inhomogeneous electric field strength and the variation in dielectric constant with temperature and density.

For two-phase flows, the dielectrophoretic force dominates because the gradient in the dielectric permittivity, $\nabla\varepsilon$, is very high at the vapor–liquid interface resulting in a large EHD force acting on the interface. This force can cause interfacial instabilities that force the liquid with higher permittivity to move to the regions of higher electric field. This phenomenon is usually referred to as the liquid extraction phenomena [9,11], and is believed to be the

primary mechanism responsible for flow regime transition causing heat transfer enhancement during EHD augmented two-phase flows.

In this work, an experimental investigation has been performed to study how variations in the mass flux, the inlet quality and the level of applied voltage influence the heat transfer and pressure drop characteristics of in-tube convective condensation of refrigerant HFC-134a.

2. Experimental facilities and methodology

The experimental test facility developed for convective boiling experiments in [23–25] was modified for the present study of convective condensation and is shown schematically in Fig. 1. The facility consists of a closed loop charged with refrigerant HFC-134a. The main components of the loop are the gear pump, electrically heated sections, water heated section, test section, condenser and pressurizer along with various measuring devices. Refrigerant is circulated throughout the loop by a gear pump located at the exit of the condenser. The refrigerant inlet quality to the test section can be controlled by two separate heating sections; direct electric heating and water heating in a plate-type heat exchanger. The refrigerant exiting the heat exchanger is directed into the horizontal test section via a straight length of 0.55 m (50 diameters) tubing to achieve fully developed conditions. Leaving the test section, the refrigerant enters a 30 kW co-axial single-pass condenser to return the refrigerant two-phase mixture exiting the test section to its original liquid state before entering the pump. The test section consists of a single tube counter-current heat exchanger as depicted in Fig. 2. The electric field is established by connecting a high voltage source to the concentric electrode while the tube side surface is grounded. The top and bottom surface temperatures of the test section tube are measured using 0.5 mm diameter T-type thermocouples embedded in $0.5\,\text{mm} \times 0.5\,\text{mm} \times 2.5\,\text{mm}$ grooves along the axial direction for estimating the average heat transfer coefficient on the refrigerant side of the heat exchanger. These measurements were also used to identify the flow regimes inside the tube. Excluding the thermal resistance of the stainless tube [23–25] and assuming that the average heat transfer coefficient is uniform both axially and circumferentially, the refrigerant side average heat transfer coefficient in the tube can be approximated as

$$\overline{h}_{\text{i}} = \frac{Q_{\text{w}}}{S_{\text{i}}\left(T_{\text{sat}} - T_{S_{\text{avg}}}\right)} \tag{2}$$

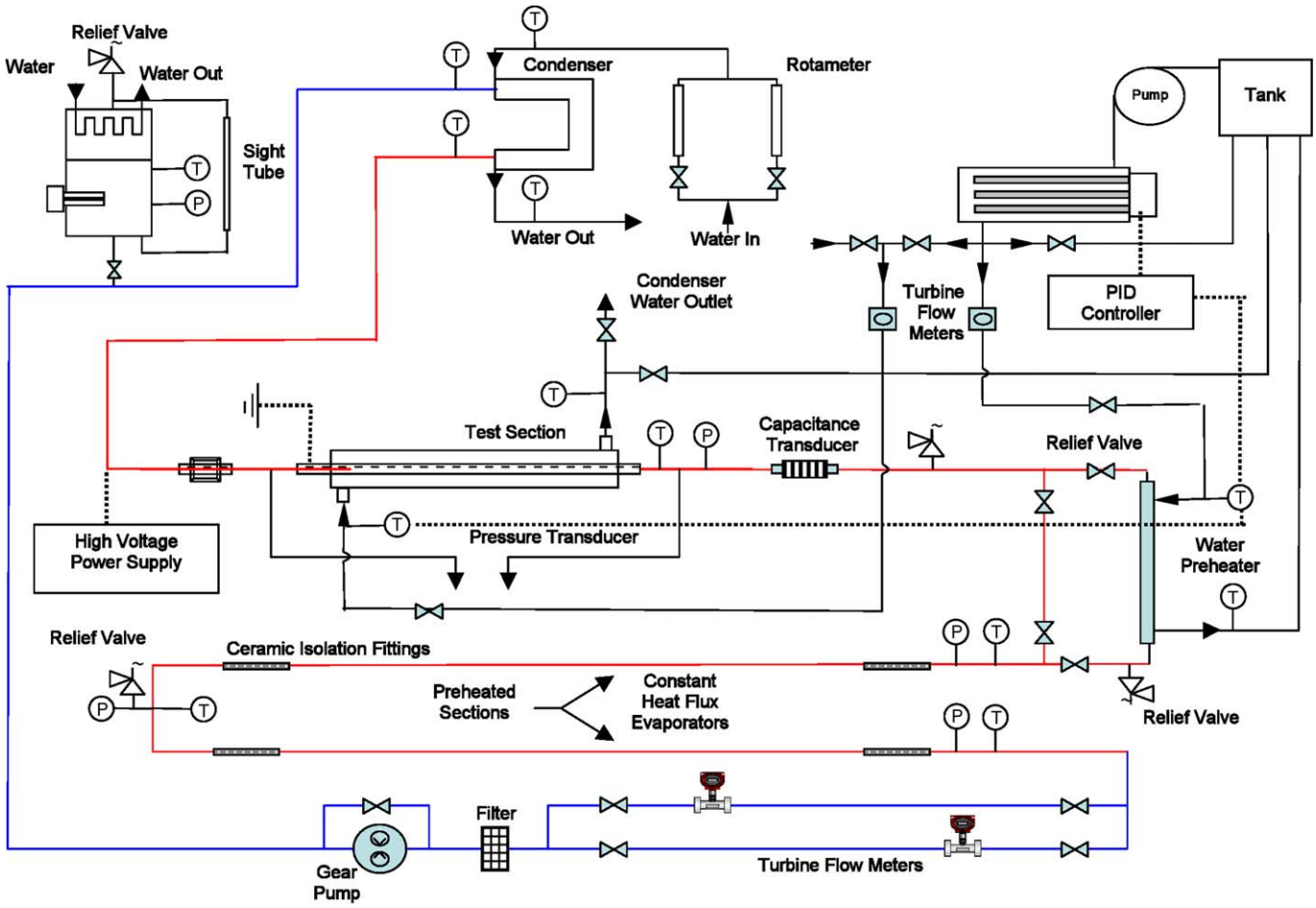

Fig. 1. Schematic diagram of test facility.

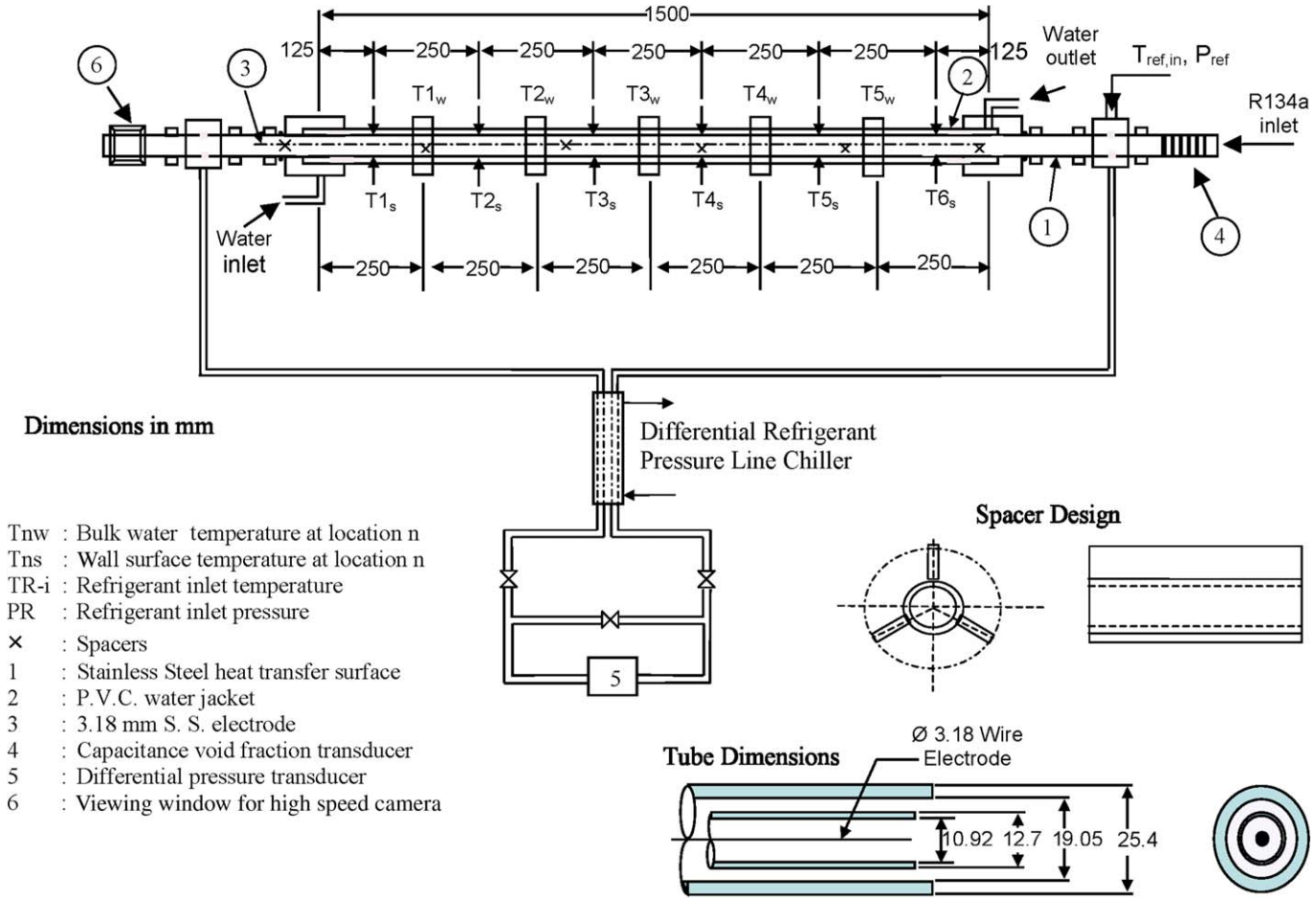

Fig. 2. Schematic diagram of the test section.

where S_i is the inner surface area of the stainless steel tube, T_{sat} is the refrigerant saturation temperature, and Q_w is the heat extracted by the coolant water from the condensing refrigerant within the test section;

$$Q_w = \dot{m}_w c_{pw}(T_{w-o} - T_{w-i}) \quad (3)$$

The arithmetic average of the surface temperature, $T_{S_{avg}}$, was obtained according to

$$T_{S_{avg}} = \frac{1}{12}\sum_{1-t,b}^{6-t,b} Ti_{S-t,b} \quad (4)$$

For the sake of confirming the accuracy of the experimental measurements the power extracted from the refrigerant by the condenser and the test section was compared with the total power input by the preheaters and the surroundings as follows:

$$Q_{out} = Q_w + Q_{cond} \quad (5)$$

$$Q_{in} = Q_{PRE} + Q_{surr} \quad (6)$$

where Q_{cond}, Q_{PRE}, and Q_{surr} are given by

$$Q_{cond} = \dot{m}_{w-cond} c_{pw}(T_{w-cond,o} - T_{w-cond,i}) \quad (7)$$

$$Q_{PRE} = [I(V_1 + V_2)] + \left[\dot{m}_{w-PRE} c_{pw}(T_{w-PRE-i} - T_{w-PRE-o})\right] \quad (8)$$

$$Q_{surr} = \dot{m}_{ref} c_p (T_{R-Sub} - T_{R-Cond-0}) \quad (9)$$

Table 1
Experimental uncertainty

Parameter	Uncertainty
Temperature, T	±0.1 °C
Mass flow rate, $\dot{m}$	±0.00004 kg/s ($\dot{m} < 0.02$ kg/s)
	±0.0001 kg/s (0.028 kg/s $< \dot{m} <$ 0.28 kg/s)
Pressure drop, ΔP	±8 Pa
Applied voltage, V	±0.2 kV
Heat flux, q'' (W/m^2)	±10%
Heat transfer coefficient, h (W/m^{2}K)	±14%
Quality	±6%

The energy balance was found to be within ±10% for all the conditions tested which provides confidence in the efficacy of the measurement and analysis techniques used in this investigation.

The experimental uncertainties for the measured and calculated parameters are summarized in Table 1.

3. Results and discussion

The effects of varying the mass flux, the inlet quality and the level of applied voltage are examined in this investigation. The ranges of experimental conditions are listed in Table 2.

Table 2
Experimental text conditions

	EHD voltage, V (kV)	Mass flux, G (kg/m^2 s)	Heat flux, q'' (kW/m^2)	Inlet quality, x_{in}
Effect of mass flux, $\dot{m}$	0, 8	56–264	9.6	67%
Effect of inlet quality, x_{in}	0, 8	74	9.6	59–83%
	0, 8	240	9.6	20–64%
Effect of EHD voltage, V	0–8	83.4	10.2	66%

3.1. Effect of mass flux

In order to elucidate the influence of an electric field on the flow regime and associated heat transfer performance for condensing two-phase flow, experiments were performed whereby the inlet quality and heat flux were held constant and the refrigerant mass flux was varied between $G = 55$ kg/m^2 s and $G = 263$ kg/m^2 s for two levels of applied voltage, $V = 0$ kV and $V = 8$ kV. Changes in the overall heat transfer coefficient and flow regime are interpreted with reference to the corresponding variations of the top and bottom surface temperatures of the test section as well as changes in the measured pressure drop across the test section length.

Fig. 3 shows the range of the current experimental conditions on the Steiner flow regime map as modified by Cotton [23] for the annular geometry in this investigation for the no applied voltage case. According to this estimation, stratified flow is to be expected along the entire test section length for the lower mass flux settings. A transition to annular flow is expected to occur as the mass flux is increased.

3.1.1. Identification of flow regimes with and without EHD

The top and bottom local surface temperature profiles for different mass flux settings are depicted in Fig. 4 without an electric field for a constant inlet quality and heat flux. Fig. 4a shows that there is no distinct difference between the surface subcooling measurements along the top surface for each mass flux tested. This result implies that there is always a film of liquid condensate of nearly uniform thickness at the top of the tube. Along the bottom of the test section, Fig. 4b shows a general trend of increasing surface subcooling along the length of the test section for each mass flux tested. This trend indicates that the thermal resistance, or equivalently the liquid layer thickness, increases along the test section length as vapor is condensed and pools in the lower region of the tube. For the lowest mass flux setting of $G = 55$ kg/m^2 s, the surface subcooling along the bottom is at all times considerably higher than that of the top. This indicates that the flow is in the stratified regime along the entire length. This observation is consistent with the prediction of the flow map given in

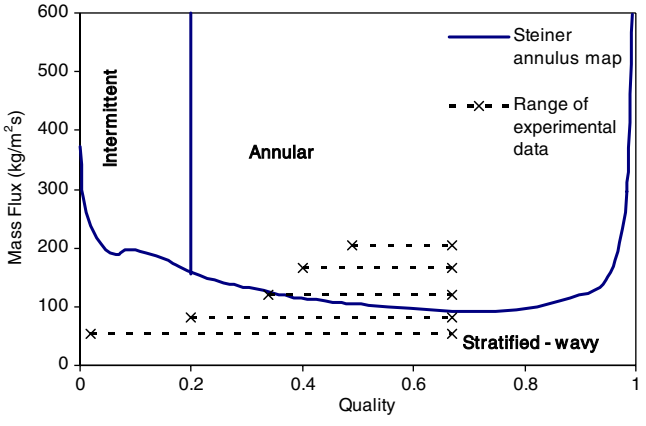

Fig. 3. Steiner flow regime map modified by Cotton [23] for annular geometries.

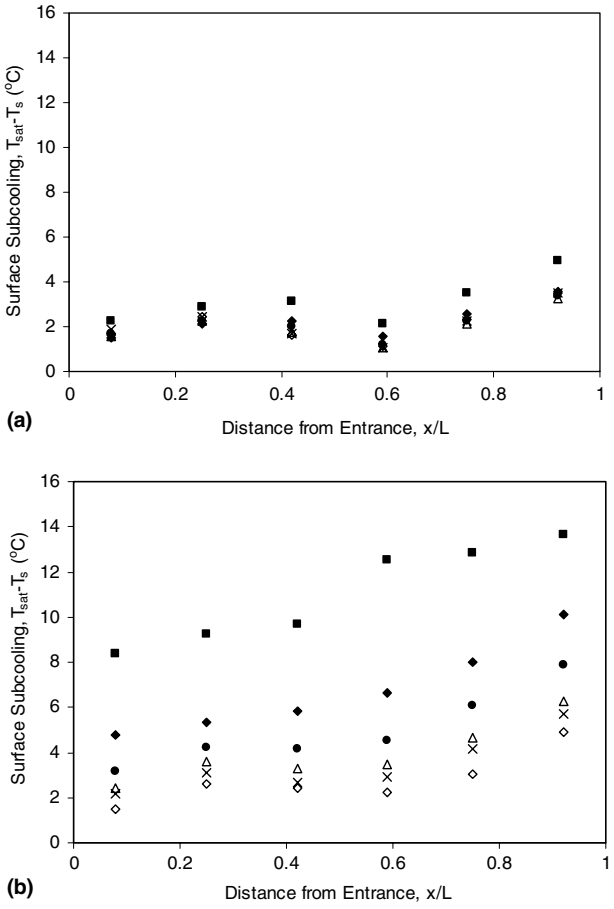

Fig. 4. Time-averaged surface subcooling profiles for varying mass flux and constant heat flux of $q'' = 9.6$ kW/m^2 and inlet quality of $x_{in} = 67\%$ without EHD: (a) top surface, (b) bottom surface. ■ $G = 55$ kg/m^2 s ($X_{out} = 5\%$, $\alpha = 30\%$), ● $G = 82$ kg/m^2 s ($X_{out} = 20\%$, $\alpha = 68\%$), ◆ $G = 120$ kg/m^2 s ($X_{out} = 35\%$, $\alpha = 78\%$), △ $G = 160$ kg/m^2 s ($X_{out} = 40\%$, $\alpha = 80\%$), × $G = 200$ kg/m^2 s ($X_{out} = 50\%$, $\alpha = 85\%$), ◇ $G = 263$ kg/m^2 s ($X_{out} = 50\%$, $\alpha = 85\%$).

Fig. 3. As the mass flux increases, the bottom surface subcooling becomes progressively lower at each measurement point indicating that the liquid layer thickness, and thus the level of stratification, decreases with increasing mass flux. For the highest mass flux tested, $G = 263\ \mathrm{kg/m^2\,s}$, the temperature measurements along the top and bottom are similar enough to conclude that a film of nearly uniform thickness exists around the periphery of the tube. Here the flow regime is annular with entrained droplets likely to be present in the vapor core. The appearance of annular flow at both the inlet and outlet of the test section is consistent with the prediction of the flow map given in Fig. 3 for high mass flux.

The top and bottom local surface temperature profiles for different mass flux settings are depicted in Figs. 5 and 6 for two levels of applied voltage, $V = 0$ kV (top graphs) and $V = 8$ kV (bottom graphs). Once again, the inlet quality and heat flux are constant so as to elucidate the effects of mass flux and voltage level on the flow regime and heat transfer. For the lower range of mass flux, $G = 55\ \mathrm{kg/m^2\,s}$ to $G = 120\ \mathrm{kg/m^2\,s}$, Fig. 5 indicates that increasing the mass flux and applying the electric field have little influence on the temperature along the top surface of the tube. This is not the case along the bottom of the tube where there is a significant influence on the temperature profiles. Considering Fig. 5a, the top graph shows that without the application of the electric field the flow is stratified with a thin liquid layer in the upper region of the tube and a thick liquid layer in the bottom region that becomes thicker along the heat exchanger length as vapor continuously condenses to liquid. However, with the application of an electric field the top and bottom wall surface temperatures are nearly equal at the high quality region of the test section inlet. This suggests that the flow regime is annular-mist with a nearly uniform annular film thickness. In this instance, it is likely that the EHD force is strong enough to extract most of the liquid stratum at the bottom of the tube into the vapor core. This can be supported using an order of magnitude analysis based on the analogy to free convective flows. Cotton et al. [26] argued that the effect of the dielectrophoretic forces are significant for $(M_d/Re_l^2) > 0.1$, where Re_l is the liquid Reynolds number and M_d is the Masuda number or the dielectric Rayleigh number. In the current experiments, the ratio (M_d/Re_l^2) is of order one for an applied voltage of 8 kV, which suggests that the dielectrophoretic forces can be significant compared to the inertial forces. Further along the test section the quality decreases due to condensation of the vapor. Approximately midway along its length, the bottom surface subcooling begins to increase at such a rate that the temperature approaches the $V = 0$ kV case at the exit. This indicates that as the local liquid volume in the test section increases beyond a certain value along its length, the effect of EHD diminishes. This is likely due to the liquid in the stratified layer coming into contact with the electrode, which reduces the effect of EHD on the interface until it can no longer influence a transition in the flow regime. This is supported by the low quality ($x = 0.05$) at the outlet for this case.

For a mass flux of $G = 82\ \mathrm{kg/m^2\,s}$, Fig. 5b indicates that with the application of EHD, the flow regime along the entire test section changes from stratified to annular-mist flow. The test section quality range for this case is $0.2 \leqslant x \leqslant 0.67$ and will be considered the maximum enhancement region for this investigation. In this quality range, it is likely that the electric body force is strong enough to overcome the restoring forces and cause a flow regime transition for each mass flux tested. Fig. 5c illustrates that as the mass flux is increased to $G = 120\ \mathrm{kg/m^2\,s}$, the top and bottom surface subcooling profiles without EHD begin to converge and the flow regime is transitioning from stratified to annular flow. The surface subcooling measurements indicate that the application of EHD still causes flow regime transition to annular flow

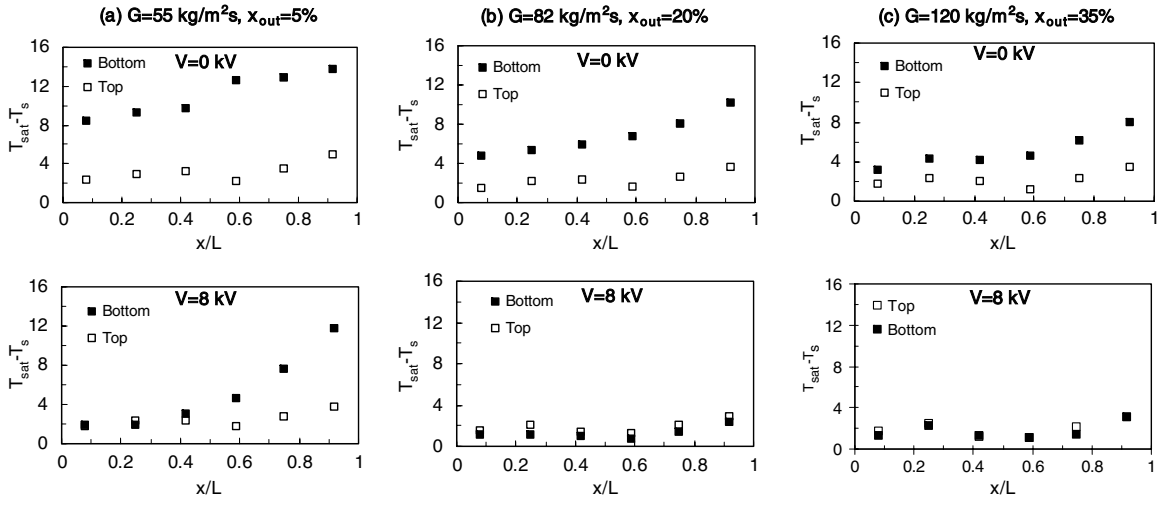

Fig. 5. Time-averaged surface subcooling profiles for mass flux levels where EHD has a significant influence on the flow regime and heat transfer coefficient. Measurements taken for a constant heat flux of $q'' = 9.6\ \mathrm{kW/m^2}$ and inlet quality of $x_{in} = 67\%$ both with and without EHD.

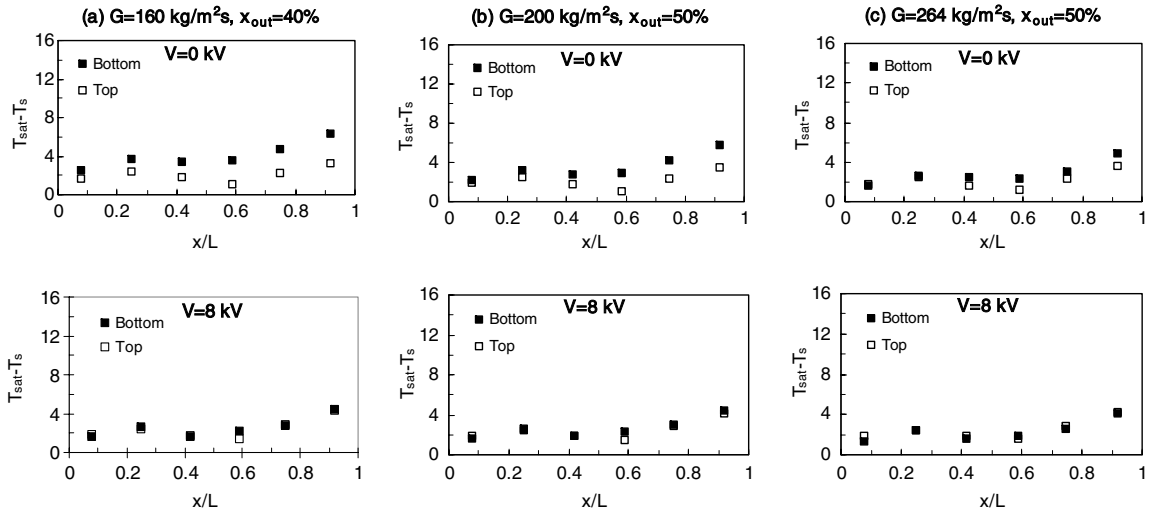

Fig. 6. Time-averaged surface subcooling profiles for mass flux levels where EHD does not have a significant influence on the flow regime and heat transfer coefficient. Measurements taken for a constant heat flux of $q'' = 9.6\ \mathrm{kW/m^2}$ and inlet quality of $x_{in} = 67\%$ both with and without EHD.

with an approximately uniform film. Once again, the quality range for this case is within the maximum enhancement region so that the application of EHD causes transition to annular flow along the entire length of the test section.

Without EHD, increasing the mass flux causes the annular film to become progressively thinner and circumferentially more uniform. This is illustrated in Fig. 6a–c where it is noticed that the surface subcooling profiles for the top and bottom converge to the point where differences are small enough that the flow can be considered annular. Here, the effect of EHD on the top and bottom surface temperatures becomes less noticeable with further increase in the mass flux, as illustrated in the bottom graphs in Fig. 6. It is conjectured that by increasing the mass flux, the bottom liquid stratum begins to wash up around the tube wall such that the distance between the charged electrode and the vapor–liquid interface increases. At this point the vapor–liquid interface is far enough away from the electrode that the EHD forces are no longer strong enough to extract sufficient liquid into the core to have as noticeable an influence on the flow regime.

3.1.2. Heat transfer and pressure drop results

A flow regime transition has a direct influence on the heat transfer coefficient on the refrigerant side of the heat exchanger. As discussed, the application of EHD can have the effect of changing the flow field from the stratified flow regime to the annular flow regime. The thermal resistance to heat transfer can be conceptualized as being proportional to the liquid layer thickness for conduction across a liquid film. Therefore, upon applying EHD the reduction in the liquid film thickness in the bottom region due to the liquid extraction phenomena results in a net decrease in the thermal resistance to heat transfer with a subsequent increase in the heat transfer coefficient.

The effect of EHD on the heat transfer performance for varying mass flux is shown in Fig. 7. The figure indicates

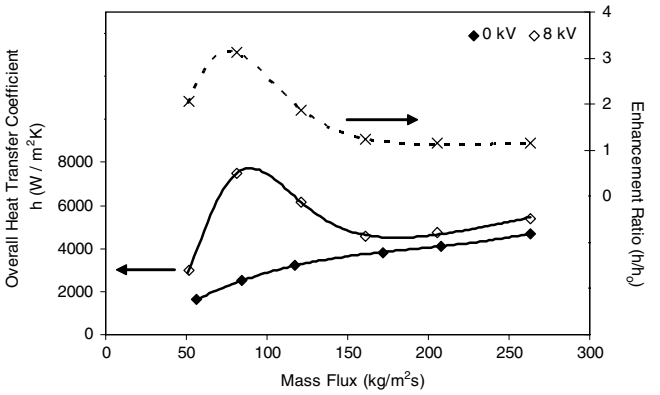

Fig. 7. The effect of mass flux on the refrigerant side overall heat transfer coefficient for $V = 0\ \mathrm{kV}$ and $V = 8\ \mathrm{kV}$ and the enhancement ratio. Measurements taken for a constant heat flux of $q'' = 9.6\ \mathrm{kW/m^2}$ and inlet quality of $x_{in} = 67\%$.

that in the region $G \leqslant 85\ \mathrm{kg/m^2\,s}$, the augmented heat transfer coefficient, h, and the enhancement ratio, h/h_o, increases with increased mass flux. Increasing the mass flux for constant heat addition and inlet quality has the effect of increasing the outlet quality such that a larger portion of the test section has a quality which lies within the maximum enhancement region. This means that a larger portion of the tube will experience flow regime transition from stratified to annular flow thus increasing the average heat transfer coefficient of the test section. For mass flux levels between $85\ \mathrm{kg/m^2\,s} \leqslant G \leqslant 150\ \mathrm{kg/m^2\,s}$, Fig. 7 shows a decrease in the augmented heat transfer coefficient as well as the enhancement ratio with further increase of the mass flux. Since the vapor–liquid interface is moving further out from the electrode as the flow becomes more annular, the influence of EHD on the flow regime transition and heat transfer performance becomes less pronounced. When the base flow is annular, such as for the case $G \geqslant 150\ \mathrm{kg/m^2\,s}$, the influence of EHD diminishes to such an extent that

only slight changes in the liquid layer thickness and associated heat transfer performance are realized. Here, the enhancement ratio remains nearly constant at $h/h_o \approx 1.15$.

The current experimental results are compared to the results of Gidwani et al. [18] in Fig. 8. While the test conditions are not identical, Gidwani et al. [18] used a similar heat exchanger/electrode geometry in the same mass flux range. The comparison shows similar trends in the heat transfer enhancement with the mass flux. However, the enhancement levels obtained by Gidwani et al. [18] are higher at the larger mass flux. This is likely due to the lower average quality in the experiments of Gidwani et al. [18], where the quality was 30% compared to 50% in the present case. At high mass flux, increasing the inlet quality results in thinner liquid films, with a consequent decrease in the enhancement level due to the EHD. It should also be noted that Gidwani et al. [18] used refrigerants R404 and R407, while the present experiments were performed with R134a.

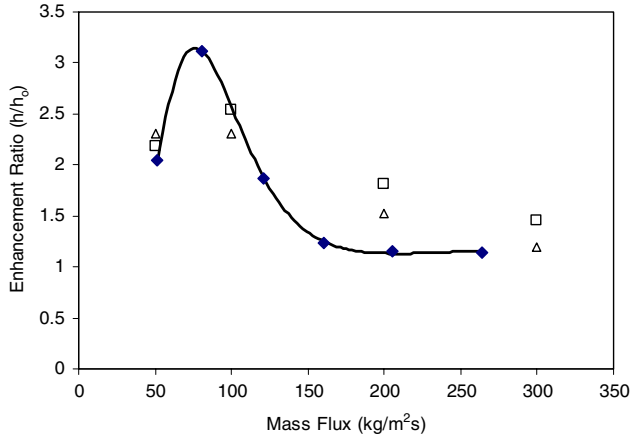

Fig. 8. The effect of mass flux on the enhancement ratio. Measurements taken for a constant heat flux of $q'' \approx 10$ kW/m^2. ♦ Present data $x_{in} = 67\%$, $x_{ave} = 50\%$; □ Gidwani et al. [18] $x_{ave} = 30\%$-R404a; △ Gidwani et al. [18] $x_{ave} = 30\%$-R407c.

There is a pressure drop penalty associated with application of EHD as revealed in Fig. 9. It is speculated that the increase in the pressure drop due to the application of EHD is primarily due to the destabilization of the boundary layer near the outer tube wall and increased wall shear stress on the electrode due to liquid droplet impingement on the electrode surface. Under the influence of an electric field, liquid is extracted from the bottom stratum into the vapor core. This causes secondary motions in the liquid stratum which disturbs the liquid boundary layer near the wall causing higher wall shear stresses. Thinning of the liquid layer thickness can also increase the velocity gradient at the wall and consequently increase the wall shear stress at the outer tube surface. The continuous interaction between the entrained droplets and the concentric electrode are also likely to increase the shear stress at the electrode wall adding to the overall increase in the pressure drop observed in Fig. 9.

3.2. Effect of inlet quality

The effect of EHD on the heat transfer coefficient and pressure drop for the case of increasing inlet quality for a fixed heat flux of $q'' = 9.6$ kW/m^2 and two levels of mass flux, $G = 74$ kg/m^2 s (stratified flow) and $G = 240$ kg/m^2 s (annular flow), are illustrated in Figs. 10–12. For the low mass flux-stratified flow case shown in Fig. 10, it is evident that the application of EHD enhances the heat transfer coefficient for the entire range of inlet qualities tested, $60\% \leqslant x_{in} \leqslant 80\%$. Analysis of the top and bottom surface temperature profiles (not shown) revealed that the increased heat transfer can once again be attributed to flow regime transition from stratified flow to annular flow over a portion or the entire length of the test section depending on the local quality. For inlet quality in the range of $60\% \leqslant x_{in} \leqslant 72\%$ the test section exit quality is in the range of $7\% \leqslant x \leqslant 18\%$ which lies outside the maximum enhancement region such that EHD has a relatively weak

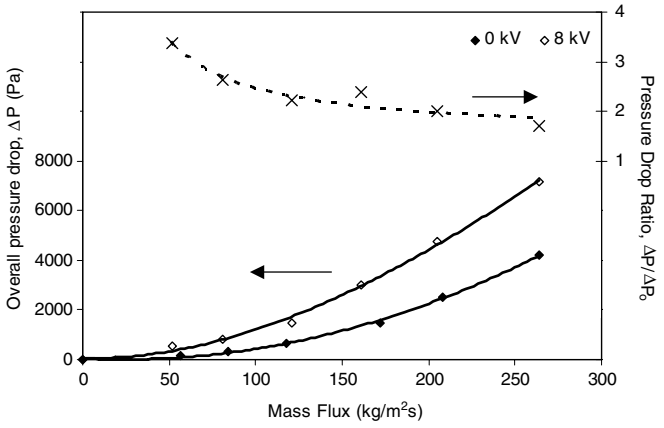

Fig. 9. The effect of inlet quality on the refrigerant side overall heat transfer coefficient for $V = 0$ kV and $V = 8$ kV and the enhancement ratio. Measurements taken for a constant heat flux of $q'' = 9.6$ kW/m^2 and inlet quality of $x_{in} = 67\%$.

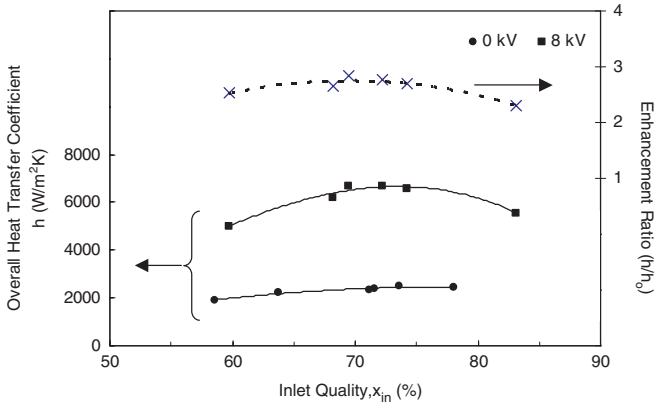

Fig. 10. The effect of inlet quality on the refrigerant side overall heat transfer coefficient for $V = 0$ kV and $V = 8$ kV and the enhancement ratio. Measurements taken for a constant heat flux of $q'' = 9.6$ kW/m^2 and mass flux $G = 74$ kg/m^2 s.

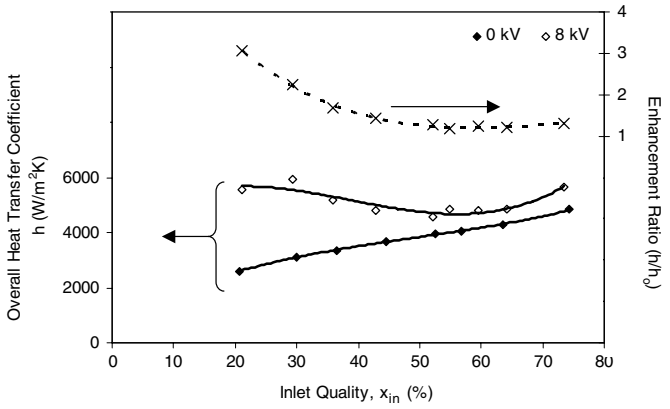

Fig. 11. The effect of inlet quality on the refrigerant side overall heat transfer coefficient for $V = 0$ kV and $V = 8$ kV and the enhancement ratio. Measurements taken for a constant heat flux of $q'' = 9.6$ kW/m^2 and mass flux $G = 240$ kg/m^2 s.

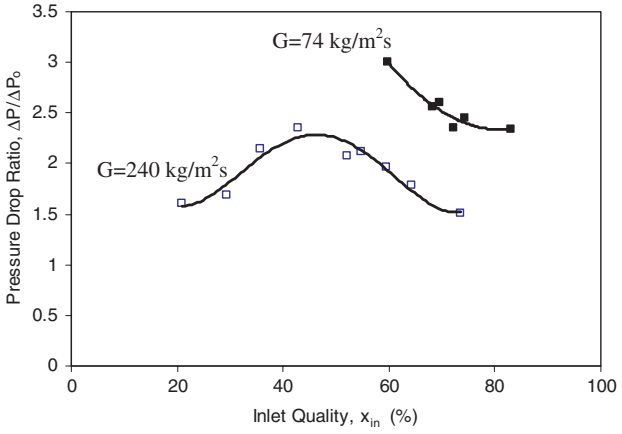

Fig. 12. The effect of inlet quality the pressure drop ratio for $G = 74$ kg/m^2 s and $G = 240$ kg/m^2 s. Measurements taken for a constant heat flux of $q'' = 9.6$ kW/m^2.

effect on the flow nearing the exit. As a result, enhancement only occurs over a portion of the test section length, and is similar to that depicted in Fig. 5a. As the inlet quality and subsequent outlet quality is increased, the heat transfer coefficient as well as the enhancement ratio increases because the flow regime transition occurs over a progressively larger portion of the test section length. The observation that the heat transfer coefficient as well as the enhancement ratio increases, reaches a maximum at $x_{in} \sim 72\%$ and begins to decrease with increasing inlet quality suggests that there is a mechanism at work that reduces the ability of EHD to reduce the liquid layer thickness. It is likely that for $x_{in} \geqslant 72\%$, increasing the inlet quality results in an overall decrease in the thickness of the liquid stratum at the bottom of the test section resulting in an interfacial electric body force that is weaker and less able to extract liquid from the stratum into the vapor core.

The effect of EHD and inlet quality on the overall heat transfer coefficient and the enhancement ratio for a mass flux of $G = 240$ kg/m^2 s and heat flux of $q'' = 9.6$ kW/m^2 is shown in Fig. 11. For this mass flux the flow regime at the inlet of the test section is very close to annular flow. As the inlet quality is increased the annular liquid film becomes more uniform as the liquid thickness in the bottom region decreases. The thinning of the liquid layer hampers the ability of the EHD to extract liquid, as previously discussed, and accounts for the decrease in the heat transfer coefficient and the enhancement ratio observed in Fig. 11. For inlet qualities greater than about 40%, the flow regime along the whole test section is annular flow prior to the application of EHD such that it has no significant effect on the heat transfer enhancement and $h/h_o \approx 1.15$, as shown in Fig. 11.

The effect of inlet quality on the overall pressure drop penalty for the cases discussed above is shown in Fig. 12. In each case there is a pressure drop penalty due to the application of EHD. As previously discussed, it is speculated that the increase in the pressure drop due to the application of EHD is primarily due to the destabilization and thinning of the boundary layer near the outer tube wall and may also be influenced significantly by liquid droplet impingement on the inner electrode. It stands to reason that the larger influence that EHD has on the flow regime transition, the higher the pressure drop penalty will be.

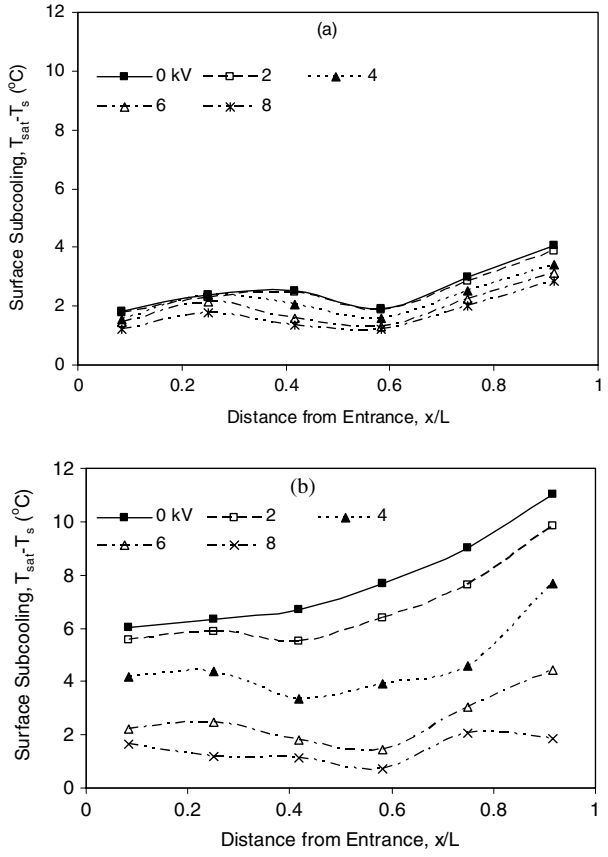

Fig. 13. Time-averaged surface subcooling profiles for varying applied voltage and constant mass flux $G = 83.4$ kg/m^2 s, heat flux of $q'' = 10.2$ kW/m^2 and inlet quality of $x_{in} = 66\%$: (a) top surface, (b) bottom surface.

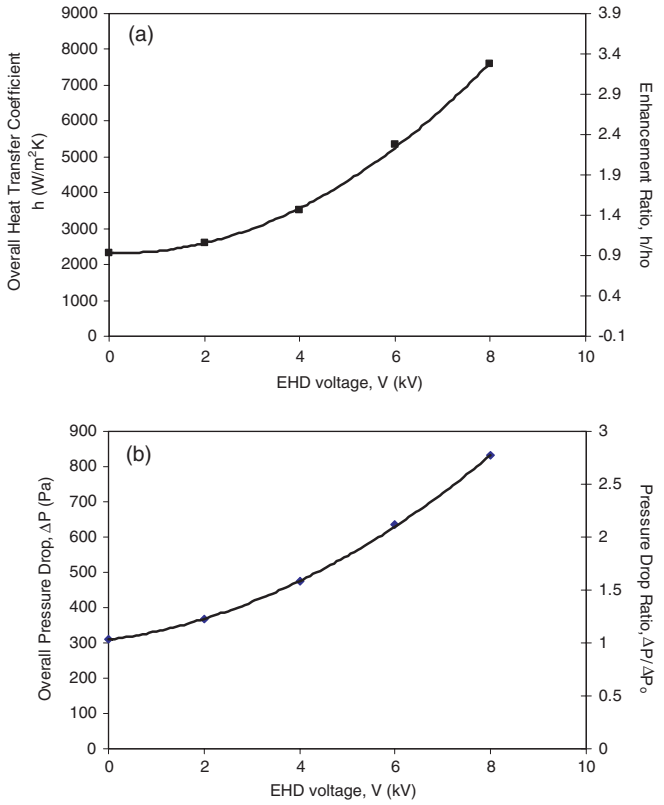

Fig. 14. Effect of varying the varying applied voltage and constant mass flux $G = 83.4\ \mathrm{kg/m^2\,s}$, heat flux of $q'' = 10.2\ \mathrm{kW/m^2}$ and inlet quality of $x_{in} = 66\%$ on (a) the heat transfer coefficient and (b) the pressure drop.

This accounts for the general observations that the pressure drop penalty is significantly higher for the $G = 74\ \mathrm{kg/m^2\,s}$ case as compared with the $G = 240\ \mathrm{kg/m^2\,s}$ case, as shown in Fig. 12. The initial upward trend for the $G = 240\ \mathrm{kg/m^2\,s}$ measurements is difficult to interpret without specific details of the flow regimes for the EHD and non-EHD cases. However, high-speed video of the flow at the exit of the test section revealed intermittent bridging of the lower liquid layer with the upper surface of the tube. It can thus be speculated that the pressure drop penalty due to EHD in this regime is less significant than that for annular and stratified flows since the wetted area within the tube is greater for the intermittent flow regime. By increasing the inlet quality, the length of the test section over which the flow is intermittent decreases and therefore the pressure drop penalty increases. Once $x_{in} > 40\%$, the flow along the entire test section is in the annular flow regime. Increasing the quality decreases the effect of EHD as the liquid film thickness becomes thinner and therefore decreases the pressure drop penalty.

3.3. Effect of applied EHD voltage

The effect of increasing the EHD voltage for fixed mass flux of $G = 83.4\ \mathrm{kg/m^2\,s}$, heat flux of $q'' = 10.2\ \mathrm{kW/m^2}$, and inlet quality of $x_{in} = 66\%$ is presented in Figs. 13 and 14. Increasing the applied voltage level strengthens the electric field acting within the phases and at the interfacial region. Assuming liquid extraction is the dominant mechanism acting to augment the flow, the higher electric field strength will result in more liquid being removed from the liquid film and into the vapor core. The top and bottom surface subcooling temperature profiles shown in Fig. 13 are consistent with this supposition. Increasing the applied voltage causes both the top and bottom surface subcooling measurements to decrease signifying that the liquid layer becomes progressively thinner thus decreasing the thermal resistance across the layer. The effect is more pronounced along the bottom region where the vapor–liquid interface is closer in proximity to the electrode. Due primarily to the thinning of the bottom liquid stratum, the heat transfer coefficient increases with increasing voltage as shown in Fig. 14a. Likewise, the pressure drop increases since the higher voltage levels have a more disruptive influence on the flow as illustrated in Fig. 14b. The maximum EHD power consumption is less than 3 W for any flow condition, which is less than 0.53% of the applied heat flux (0.57 kW).

4. Conclusions

The experiments conducted for condensing two-phase flow in an annular channel under the influence of an electric field provide evidence that the EHD force is strong enough to extract sufficient liquid from the liquid stratum at the bottom region of the tube to cause flow regime transition from stratified flow to annular flow. The decrease in the liquid layer thickness and introduction of droplets into the vapor core result in an increase in the heat transfer coefficient of the heat exchanger together with an increase in the measured pressure drop across the test section. Measurements taken for a constant heat flux of $q'' = 9.6\ \mathrm{kW/m^2}$ and inlet quality of $x_{in} = 67\%$ reveal that for a mass flux of $82\ \mathrm{kg/m^2\,s}$ the heat transfer coefficient and pressure drop increase by approximately 3 times with the application of $V = 8\ \mathrm{kV}$. If the mass flux and/or quality are high enough for the base flow to be annular the effect of EHD on the heat transfer and pressure drop is less noticeable because for annular flow the thin liquid film is far enough away from the electrode that the EHD forces are diminished. The effect of increasing the applied voltage level is a progressive decrease in the bottom liquid layer thickness with an associated decrease in the wall temperature and increase in heat transfer coefficient and pressure drop. For a constant mass flux of $G = 83.4\ \mathrm{kg/m^2\,s}$, heat flux of $q'' = 10.2\ \mathrm{kW/m^2}$ and inlet quality of $x_{in} = 66\%$ increasing the applied voltage from 0 kV to 8 kV resulted in a parabolic increase in the enhancement ratio and pressure drop ratio from 1 to approximately three.

References

[1] P.H.G. Allen, T.G. Karayiannis, Review Paper: electrohydrodynamic enhancement of heat transfer and fluid flow, Heat Recovery Systems & CHP 15 (5) (1995) 389–423.

[2] J. Seyed-Yagoobi, J.E. Bryan, Enhancement of heat transfer and mass transport in single-phase and two-phase flows with electrohydrodynamics, Adv. Heat Transfer 33 (1999) 95–186.
[3] H.R. Velkoff, J.H. Miller, Condensation of vapor on a vertical plate with a transverse electrostatic field, J. Heat Transfer, Trans. ASME, Series C 87 (1965) 197–201.
[4] H.Y. Choi, J.M. Reynolds, Study of the electrostatic effects on condensing heat transfer, Air Force Technical Report, AFFDL-TR-65-51, Air Force Flight Dynamics Laboratory, Wright-Patterson Air Force Base, Ohio, 1965.
[5] H.Y. Choi, Electrohydrodynamic condensation heat transfer, J. Heat Transfer, Trans. ASME, Series C 90 (1968) 98–102.
[6] A.B. Didkovsky, M.K. Bologa, Vapor film condensation heat transfer and hydrodynamics under the influence of an electric field, Int. J. Heat Mass Transfer 24 (5) (1981) 811–819.
[7] F.M. Joos, R.W.L. Snaddon, Electrostatically enhanced film condensation, J. Fluid Mech. 156 (1985) 23–38.
[8] M.K. Bologa, I.K. Savin, A.B. Didkovsky, Electric-field-induced enhancement of vapor condensation heat transfer in the presence of a non-condensable gases, Int. J. Heat Mass Transfer 30 (8) (1987) 1577–1585.
[9] A. Yabe, K. Kikuchi, T. Taketani, Y. Mori, K. Hijikata, Augmentation of condensation heat transfer by applying non-uniform electric fields, heat transfer 1982, Hemisphere 5 (1982) 189–194.
[10] A. Yabe, K. Kikuchi, T. Taketani, Y. Mori, H. Maki, Augmentation of condensation heat transfer by applying electro-hydrodynamical pseudo-dropwise condensation, Proc. 8th Int. Heat Transfer Conf. (6) (1986) 2957–2962.
[11] A. Yabe, T. Taketani, K. Kikuchi, Y. Mori, K. Hijikata, Augmentation of condensation heat transfer around vertical cooled tubes provided with helical wire electrodes by applying non-uniform electric fields, heat transfer science and technology, in: Proceedings of the International Symposium, Hemisphere Publ. Corp., 1987, pp. 812–819.
[12] K. Yamashita, M. Kumagai, S. Sekita, Heat transfer characteristics of an EHD condenser, in: Proceedings of the Third ASME/JSME Joint Thermal Engineering Conference, vol. 3, 1991, pp. 61–67.
[13] M. Wawzynaik, J. Seyed-Yagoobi, Experimental study of electrohydrodynamically augmented condensation heat transfer on a smooth and enhanced tube, J. Heat Transfer 118 (1996) 499–502.
[14] K. Cheung, M.M. Ohadi, S.V. Dessiatoun, EHD-assisted external condensation of R134a on smooth horizontal and vertical tubes, Int. J. Heat Mass Transfer 42 (1999) 1747–1755.
[15] R.E. Holmes, A.J. Chapman, Condensation of Freon-114 in the presence of a strong nonuniform alternating electric field, J. Heat Transfer, Trans. ASME, Series C 92 (1970) 616–620.
[16] P. Cooper, P.H.G. Allen, The potential of electrically enhanced condensers, in: Proceedings of the 2nd International Symposium on the Large Scale Applications of Heat Pumps, York, UK, 1984, pp. 295–309.
[17] A. Singh, Electrohydrodynamic (EHD) enhancement of in-tube condensation heat transfer of alternative refrigerants R-134a in smooth and microfin tubes, ASHARE Trans. 103 (1) (1995) 813–823.
[18] A. Gidwani, M. Molki, M.M. Ohadi, EHD-enhanced condensation of alternative refrigerants in smooth and corrugated tubes, HVAC Res. 8 (2002) 219–238.
[19] Y. Feng, J. Seyed-Yagoobi, Mechanism of annular two-phase flow heat transfer enhancement and pressure drop penalty in the presence of a radial electric field-turbulence analysis, Trans. ASME 125 (2003) 478–486.
[20] J.E Bryan, J. Seyed-Yagoobi, Electrohydrodynamically enhanced convective boiling: relationship between electrohydrodynamic pressure and momentum flux rate, Trans. ASME 122 (2000) 266–277.
[21] W. Panofsky, M. Philips, Classical Electricity and Magnetism, second ed., Addison-Wesley Publ. Co., Reading, MA, 1962.
[22] J.S. Chang, A. Watson, Electromagnetic hydrodynamics, IEE Trans. Dielectric Elec. Insu. 1 (5) (1994) 871–895.
[23] J.S. Cotton, Mechanisms of electrohydrodynamic (EHD) flow and heat transfer in horizontal convective boiling channels, PhD Thesis, McMaster University, Hamilton, Canada, 2000.
[24] C. Norris, J.S. Cotton, M. Shoukri, J.S. Chang, T. Smith-Pollard, Electrohydrodynamic effects on flow redistribution and convective boiling in horizontal concentric tubes, ASHRAE Trans. 105 (1) (1999) 222–236.
[25] J.S. Cotton, M. Shoukri, J.S. Chang, T. Smith-Pollard, Electrohydrodynamic (EHD) flow and convective boiling augmentation in single-component horizontal annular channels, in: 2000 International Mechanical Engineering Congress and Exposition, HTD-366-4, 2000, pp. 177–184.
[26] J.S. Cotton, A.J. Robinson, M. Shoukri, J.S. Chang, A two-phase flow pattern map for annular channels under a DC applied voltage and application to electrohydrodynamic convective boiling analysis, Int. J. Heat Mass Transfer 48 (2005) 5563–5579.